J IRAN CHEM SOC
DOI 10.1007/s13738-017-1046-8

ORIGINAL PAPER

# Schiff base complex of Mo supported on iron oxide magnetic nanoparticles ($Fe_3O_4$) as recoverable nanocatalyst for the selective oxidation of sulfides

**Milad Aghajani**[1] · **Niaz Monadi**[1]

Received: 20 August 2016 / Accepted: 2 January 2017


**Abstract** In this work, a new tridentate Schiff base dioxomolybdenum(VI) complex immobilized on silica-coated magnetic nanoparticles ($MoO_2$5CML–$Fe_3O_4$@$SiO_2$) has been synthesized and characterized using different techniques such as FTIR, TGA, AAS, ICP–AES, XRD, VSM, EDX and SEM analyses. The catalytic activity of synthesized complex was examined in the oxidation of various sulfides in the presence of $H_2O_2$ as cheap, green and eco-friendly oxidant. This catalytic system provides high conversion and selectivity toward either sulfoxides or sulfones under different conditions. Also, the nanocatalyst could be easily separated and regenerated from reaction media by external magnet and could be reused for ten times without significant loss of the activity and selectivity.

**Keywords** Molybdenum complex · Magnetic $Fe_3O_4$ · Schiff base · Sulfoxide and sulfone · Hydrogen peroxide

## Introduction

Green nanotechnology is a bridge between green chemistry and nanotechnology that refers to the use of nanotechnology in order to enhance the eco-friendly processes producing negative externalities. This nanoscience has caused a fundamental change due to its direct implications on human health and environment [1–3]. The recent advancement in green nanotechnology led to potential applications of magnetic nanoparticles for the development of various applications including nanocatalysis [4], sensors [5], biomedicine [6], energy storage [7] and drug delivery [8]. In the field of catalysis, core–shell iron oxide magnetic nanoparticles ($Fe_3O_4$) as a support have found with applications due to their unique magnetic properties such as immense surface area, easy separation from the reaction mixture by external magnetic field rather than filtration or centrifugation, enhancing the contact between reactants and catalyst and finally recoverable without losing their activity and selectivity [9–11]. Magnetic nanocatalysts have been used in many organic reactions [12–17] that one of which involves the oxidation of sulfides. The selective oxidation of organic sulfides as environmental pollutants into the corresponding sulfoxides has been an attractive and important challenge in synthetic organic chemistry, since sulfoxides as biologically significant molecules are important intermediates in the synthesis of pharmaceuticals, agrochemicals and other fine chemicals [18–20]. Moreover, a basic obstacle during the oxidation of sulfides is overoxidation of the sulfoxides to their corresponding sulfones. Therefore, it is very important that the catalyst has a high selectivity toward sulfoxide or sulfone. According to green chemistry protocol, catalytic oxidation of sulfides with environmentally friendly oxidant has become significantly important [21–24]. Hydrogen peroxide ($H_2O_2$) is a desired oxidant because of high-efficient oxygen content, safety with low cost, readily available reagent, being eco-friendly, and also it produces water as the only by-product [25]. A variety of homogeneous transition metal catalysts are well known for the oxidation of organic sulfides [26–30], but the vast majority of these catalysts suffer from drawbacks such as difficult separation of the product from the reaction medium, deactivation, difficult recovery and recycling of the catalyst.

**Electronic supplementary material** The online version of this article (doi:10.1007/s13738-017-1046-8) contains supplementary material, which is available to authorized users.

✉ Niaz Monadi
Nimonadi@umz.ac.ir

[1] Department of Inorganic Chemistry, Faculty of Chemistry, University of Mazandaran, Babolsar, Iran

Published online: 23 January 2017

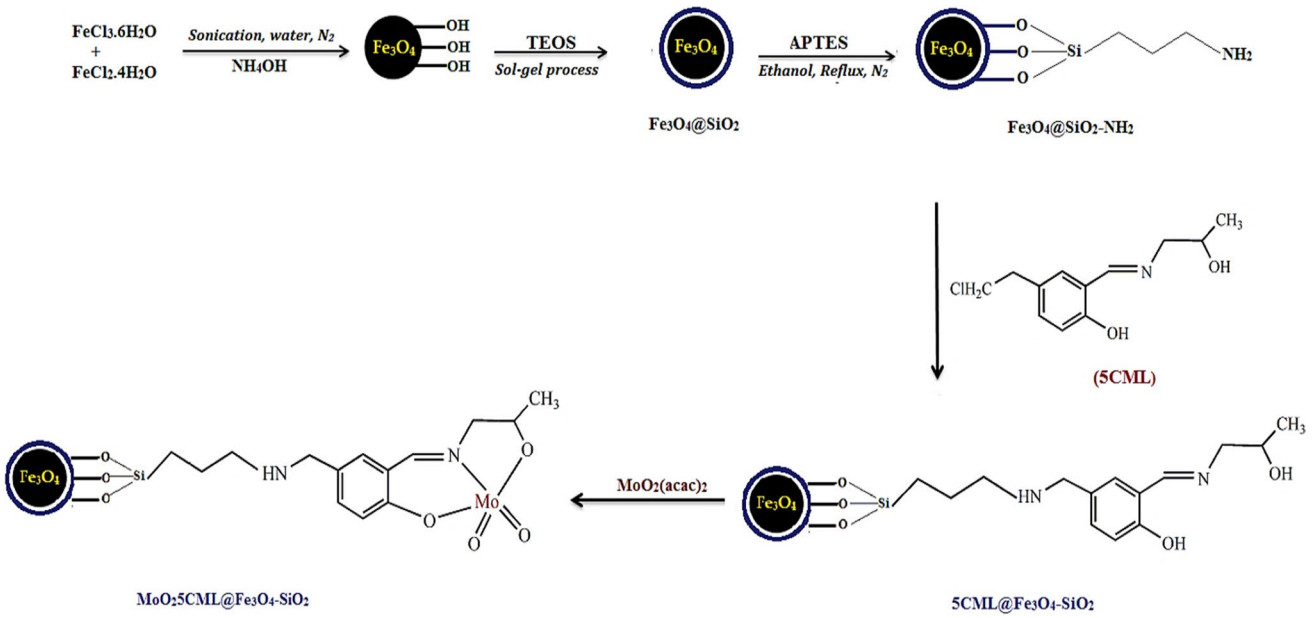


**Scheme 1** Schematic model for the preparation of catalyst

A feasible strategy to overcome these problems is to heterogenize homogeneous catalysts by anchoring them onto the convenient insoluble supports such as iron oxide magnetic nanoparticles. In this paper, a stepwise procedure is reported for the synthesis of molybdenum Schiff base complex supported on iron oxide magnetic nanoparticles modified with silica coating ($MoO_2$5CML–$Fe_3O_4$@$SiO_2$) and as an efficient, selective and recyclable catalyst for the selective oxidation of different sulfides with $H_2O_2$.

## Experimental

### Materials and methods

All reagents and solvents were procured from the commercial sources. Fourier transform infrared spectroscopy on KBr pellets of the compounds was recorded on a Bruker Vector 22 in the range of 400 and 4000 $cm^{-1}$. Elemental analyses (C, H, N) were carried out by the Elementar, Vario EL III. Mo atomic absorption spectroscopy (AAS) was performed on an Atomic Absorption Spectrometer Varian Spectra AA 110. Scanning electron microscopy (SEM) equipped with energy-dispersive X-ray spectroscopy (EDX) was carried out with a KYKY-EM3200 model. Magnetic properties of the prepared materials were measured using a homemade vibrating sample magnetometer (Meghnatis Daghigh Kavir Company, Iran) at room temperature from −10,000 to +10,000 Oe. The X-ray powder patterns (XRD) were recorded with a Bruker, D8 ADVANCE (Germany) diffractometer (CuKa radiation). The organic composition of materials and catalyst was determined by thermogravimetric analysis (TGA) and differential thermoanalysis (DTG), which was heated from 25 to 800 °C under nitrogen flow using a STA 409 PC analyzer (Netzsch). The products of the oxidation of the sulfide were determined and analyzed using a Varian CP-3800 gas chromatograph equipped with a capillary column and a flame ionization detector. The metal content of the catalysts was measured by inductively coupled plasma atomic emission analysis (ICP–AES, Varian company VISTA-PRO model).

### Synthesis

The synthesis of $MoO_2$5CML–$Fe_3O_4$@$SiO_2$ is depicted in Scheme 1 and is described as follows.

### Preparation of iron oxide magnetic nanoparticles ($Fe_3O_4$)

$Fe_3O_4$ was synthesized according to the literature with a chemical co-precipitation method [9, 10, 31]. Briefly, $FeCl_3{\cdot}6H_2O$ (21.6 mmol, 5.83 g) and $FeCl_2{\cdot}4H_2O$ (10.8 mmol, 2.147 g) were dissolved in 150 mL deionized water under constant magnetic stirring and refluxed at 85 °C under $N_2$ atmosphere. Then, 10–15 mL of $NH_3{\cdot}H_2O$ (25% w/w) was added dropwise. After continuously stirring for 2 h, the magnetite precipitates were washed by deionized water and ethanol several times. Black precipitates were collected with an external magnet and dried at 50 °C in vacuum for 12 h.

### Preparation of silica-coated $Fe_3O_4$ magnetic nanoparticles ($Fe_3O_4$@$SiO_2$)

$Fe_3O_4$@$SiO_2$ was synthesized according to the reported procedures [32, 33]. In a typical procedure, 1 g of $Fe_3O_4$ was adequately dispersed in a mixture of ethanol (70 mL) and deionized water (50 mL) for 60-min sonication at room temperature. Then, $NH_4OH$ (2.4 mL) was added to the suspension at room temperature followed by dropwise addition of tetraethyl orthosilicate (TEOS) (2 mL). After stirring at 50 °C for 2 h, the black precipitates ($Fe_3O_4$@$SiO_2$) were magnetically separated, washed with ethanol and deionized water for three times and dried in a vacuum.

### Preparation of functionalized $Fe_3O_4$@$SiO_2$ with amine groups ($Fe_3O_4$@$SiO_2$–$NH_2$)

The modification of $Fe_3O_4$@$SiO_2$ nanoparticles with 3-aminopropyltriethoxysilane (APTES) was performed in accordance with the literature in ethanol solution [34, 35]. Typically, $Fe_3O_4$@$SiO_2$ (1 g) was dispersed in 50 mL ethanol using an ultrasonic bath for 30 min. Next, APTES (2 mL) was added dropwise into the mixture under vigorous stirring and was refluxed for 12 h under $N_2$ flow. The precipitate ($Fe_3O_4$@$SiO_2$–$NH_2$) was collected by magnetic decantation and washed several times with ethanol to remove the unreacted silylating agent and finally dried at 60 °C for 6 h.

### Preparation of $Fe_3O_4$@$SiO_2$–$NH_2$-tethered 5CML (5CML–$Fe_3O_4$@$SiO_2$)

5-Chloromethyl-2-hydroxybenzaldehyde was synthesized with regard to the literature from salicylaldehyde by the classical chloromethylation method [36]. The tridentate Schiff base ligand was synthesized by addition of 5-chloromethyl-2-hydroxybenzaldehyde (5 mmol, 0.85 g) in $CH_2Cl_2$ (5 mL) to 1-amino-2-propanol (5 mmol, 0.41 g) in $CH_2Cl_2$ (5 mL). The reaction mixture was stirred for 2 h at room temperature, giving yellow oil. The oil product washed several times with $CH_2Cl_2$ and ethyl acetate. The yellow oil was denoted as 5CML. Then, $Fe_3O_4$@$SiO_2$–$NH_2$ (1 g) was dispersed in 80 mL ethanol using an ultrasonic bath for 30 min. 5CML ligand (5 mmol, 1.2 g) was added to above mixture and stirring at room temperature for 12 h under $N_2$ flow. The residual solid was filtered and washed with $CH_2Cl_2$ and ethanol and then dried in vacuum.

FTIR of 5CML: 3362 (OH); 2974, 2892 (Aliph-H); 1646 (C=N); 1259 ($CH_2$–Cl); 764 (C–Cl) $cm^{-1}$.

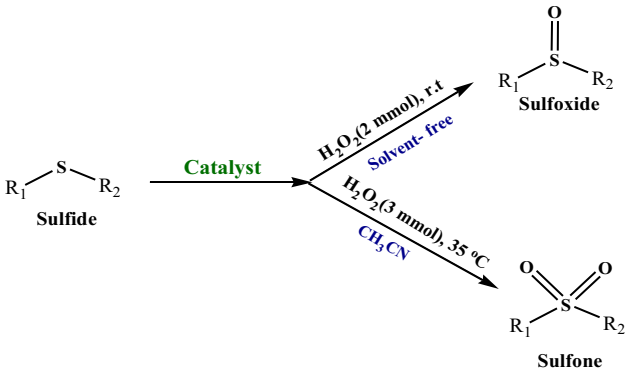


**Scheme 2** General procedure for green oxidation of sulfides

### Preparation of the nanocatalyst ($MoO_2$5CML@$Fe_3O_4$@$SiO_2$)

5CML@$Fe_3O_4$@$SiO_2$ (0.5 g) was dispersed in ethanol (50 mL), and a solution of $MoO_2(acac)_2$ (1.5 mmol, 0.49 g) in ethanol (20 mL) was added to this mixture and refluxed under $N_2$ atmosphere for 24 h. The prepared nanocatalyst was separated by magnetic decantation. To remove the unreacted $MoO_2(acac)_2$, Soxhlet extraction was carried out with ethanol, and the resulting nanocatalyst was dried under vacuum.

### General procedure for oxidation of sulfides

The oxidation of sulfides was performed in a round-bottom flask containing a mixture of sulfide (1 mmol), $H_2O_2$ (2 mmol) and catalyst (1 mol%, 17 mg based on AAS) at room temperature (Scheme 2). Progress of the reaction was monitored by TLC. After completion of the reaction, the catalyst was separated by external magnet, washed with water/ethanol and reused for subsequent recycling runs. The products were extracted by $CH_2Cl_2$. Evaporation of $CH_2Cl_2$ under vacuum gave corresponding sulfoxides or sulfones.

## Results and discussion

### Catalyst characterization

*FTIR*

The FTIR spectra of prepared materials are shown in Fig. 1. In the FTIR spectrum of $Fe_3O_4$, an intense broad peak at 577 $cm^{-1}$ is assigned as Fe–O–Fe band of $Fe_3O_4$ and a broadband around 3386 $cm^{-1}$ is due to O–H

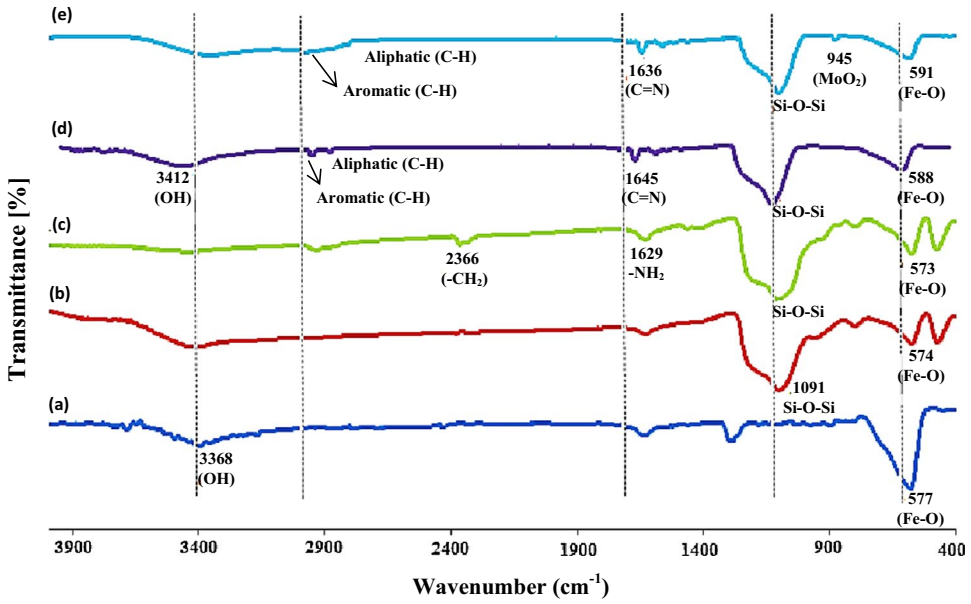


**Fig. 1** FTIR spectra for $Fe_3O_4$ (*a*), $Fe_3O_4$@$SiO_2$ (*b*), $Fe_3O_4$@$SiO_2$–$NH_2$ (*c*), 5CML–$Fe_3O_4$@$SiO_2$ (*d*) and $MoO_2$5CML–$Fe_3O_4$@$SiO_2$ (*e*)

stretching of adsorbed water (Fig. 1a). The FTIR spectrum of $Fe_3O_4$@$SiO_2$ exhibits significant reduction of the intensity of the Fe–O–Fe stretching and new peaks appear at 1091 and 800 $cm^{-1}$ corresponding to Si–O–Si and Si–OH bands, which could reveal the encapsulation of the $Fe_3O_4$ surface with the silica shell (Fig. 1b). The FTIR spectrum of $Fe_3O_4$@$SiO_2$–$NH_2$ exhibits the peaks at 2924 and 2366 $cm^{-1}$, which is ascribed to the $–CH_2$ stretching vibration aminopropyl group. Moreover, a strong band at 1629 $cm^{-1}$ corresponding to vibration mode of $–NH_2$ indicates that the aminopropyl group have successfully bonded to the surface of $Fe_3O_4$@$SiO_2$ (Fig. 1c).

Spectrum of 5CML–$Fe_3O_4$@$SiO_2$ (Fig. 1d) exhibits new absorption peaks in the 1645 $cm^{-1}$ region, which are assigned to the stretching of C=N, and some weak bands at 1550–1450 $cm^{-1}$ assigned to stretching vibrations of aromatic rings of Schiff base ligand that were not present in $Fe_3O_4$@$SiO_2$–$NH_2$ spectrum, confirming successful immobilization of ligand on $Fe_3O_4$@$SiO_2$–$NH_2$. In FTIR spectrum of $MoO_2$5CML–$Fe_3O_4$@$SiO_2$ (Fig. 1e), C=N stretching vibration (1645 $cm^{-1}$) is shifted toward the lower frequency and appeared at 1634 $cm^{-1}$, indicating coordination of C=N group of supported ligand with molybdenum center [13, 14, 36]. Also, the appearance of peak at 945 $cm^{-1}$ (stretching vibration of $MoO_2^{2+}$) is evidence of the successful grafting of metal complex on the surface of the magnetite [33].

## TGA and loading results

The TGA curves of $Fe_3O_4$, $Fe_3O_4$@$SiO_2$–$NH_2$ and $MoO_2$5CML–$Fe_3O_4$@$SiO_2$ are shown in Fig. 2.

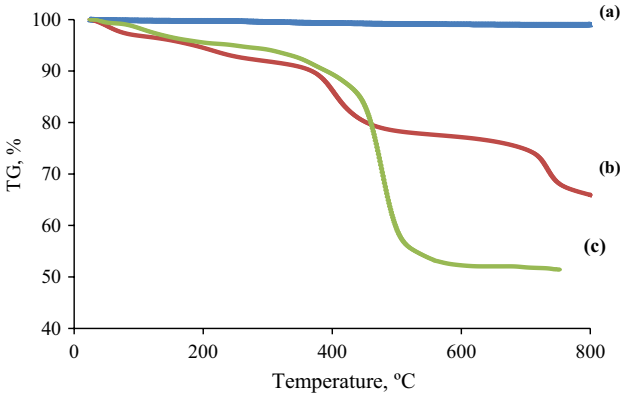


**Fig. 2** TGA analysis of $Fe_3O_4$ (*a*), $Fe_3O_4$@$SiO_2$–$NH_2$ (*b*) and $MoO_2$5CML–$Fe_3O_4$@$SiO_2$ (*c*)

The TGA curve of $Fe_3O_4$ shows a small weight loss (~2%) below 100 °C, which corresponds to the evaporation of the physically adsorbed water. As can be seen, there is no significant weight loss in the range of 100–800 °C (Fig. 2a). The TGA pattern of $Fe_3O_4$@$SiO_2$–$NH_2$ shows three weight losses at temperatures ranging from 25 to 800 °C (Fig. 2b). The first region, which is below 150 °C (~5%), is related to the evaporation of physically adsorbed solvent or trapped water. The second weight loss observed in the range of 250–450 °C (~12%) is due to decomposition of aminopropyl moieties. The third weight loss at higher temperature (above 700 °C) is resulted from the decomposition of silica shell [37]. Based on TGA analysis, the amount of loaded aminopropyl on the surface of $Fe_3O_4$@$SiO_2$ is 1.98 mmol $g^{-1}$.

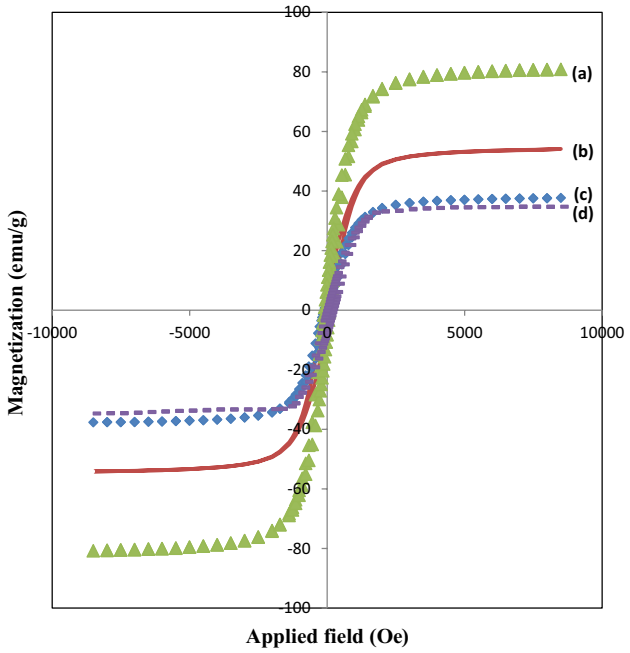


**Fig. 3** Magnetization curves obtained by VSM at room temperature for $Fe_3O_4$ (*a*), $Fe_3O_4$@$SiO_2$ (*b*), $MoO_2$5CML–$Fe_3O_4$@$SiO_2$ (*c*) and recycled catalyst after 10th run (*d*)

The TGA curve of $MoO_2$5CML–$Fe_3O_4$@$SiO_2$ is shown two weight losses (Fig. 2c). The first weight loss occurs near 150 °C that is related to the loss of trapped solvent and physically adsorbed water in complex. The second mass loss occurs at temperature range of 330–544 °C (~28%) that is corresponding to the thermal decomposition of Schiff base complex, confirming the successful grafting of complex onto the surface of $Fe_3O_4$@$SiO_2$–$NH_2$. The TGA analysis indicates that the nanocatalyst is thermally stable up to about 330 °C. The amount of loaded Schiff base complex is 0.618 mmol $g^{-1}$ based on the weight losses, which is in good agreement with the ICP–AES measurements value. The molybdenum content of nanocatalyst was found to be 0.515 mmol $g^{-1}$ based on ICP–AES analysis. The amount of loaded Mo was also measured by atomic absorption spectrophotometer (AAS) to be 0.497 mmol $g^{-1}$, which is close to ICP–AES analysis.

## VSM studies

The VSM curves of $Fe_3O_4$, $Fe_3O_4$@$SiO_2$ and $MoO_2$5CML–$Fe_3O_4$@$SiO_2$ are depicted in Fig. 3. As shown in Fig. 3, the magnetization curves exhibit no obvious remanence effect, which clearly indicates the superparamagnetic nature of the materials. The magnetization saturation values for $Fe_3O_4$, $Fe_3O_4$@$SiO_2$ and $MoO_2$5CML–$Fe_3O_4$@$SiO_2$ are 80.1, 58.3 and 36.4 emu $g^{-1}$, respectively. Compared with $Fe_3O_4$, decrease in magnetization saturation values of $Fe_3O_4$@$SiO_2$ and $MoO_2$5CML–$Fe_3O_4$@$SiO_2$ is due to the coating of $SiO_2$ shell and grafting the Schiff base metal complex on the surface of $Fe_3O_4$ [35]. The catalyst could be easily separated using an external magnet while in the absence of external magnetic field it can be well dispersed by slightly shaking, indicating that the synthesized catalyst possesses good redispersibility and magnetic responsivity (Fig. 4).

## XRD studies

The XRD pattern of $Fe_3O_4$ (Fig. 5a) shows six characteristic peaks at $2\theta = 30.2$, 35.5, 43.2, 53.6, 57.1 and 62.7°, corresponding to (220), (311), (400), (422), (511) and (440) Bragg reflections, respectively, which agrees with the standard in JCPDS card number (19-0629). The XRD pattern of $Fe_3O_4$ nanoparticles shows an inverse cubic spinel structure without any impurity. The XRD patterns of $Fe_3O_4$ (Fig. 5a) and $Fe_3O_4$@$SiO_2$ (Fig. 5b) show a new broad peak at $2\theta = 23°$–24° due to the existence of amorphous silica [38]. Moreover, the peak intensities in XRD pattern of the nanocatalyst (Fig. 5c) slightly decreased in comparison

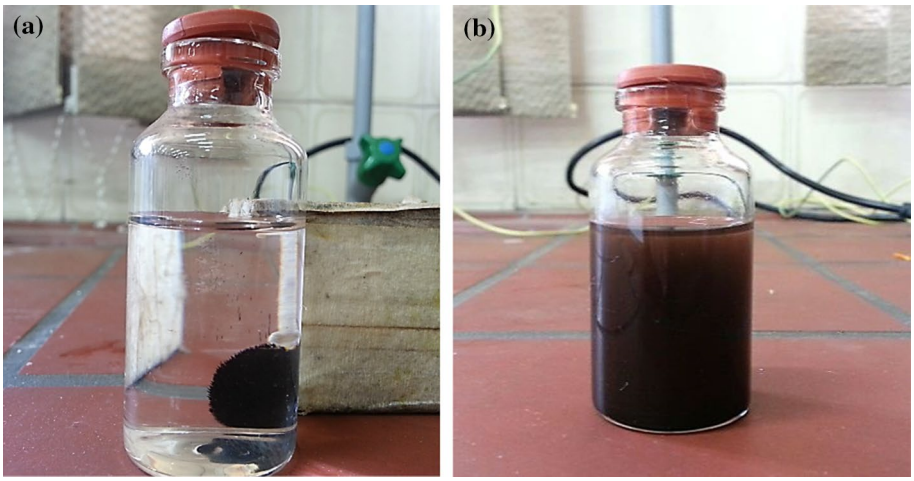


**Fig. 4** Easy separation of catalyst using an external magnet from reaction mixture (**a**) and redispersibility by slight shaking (**b**)

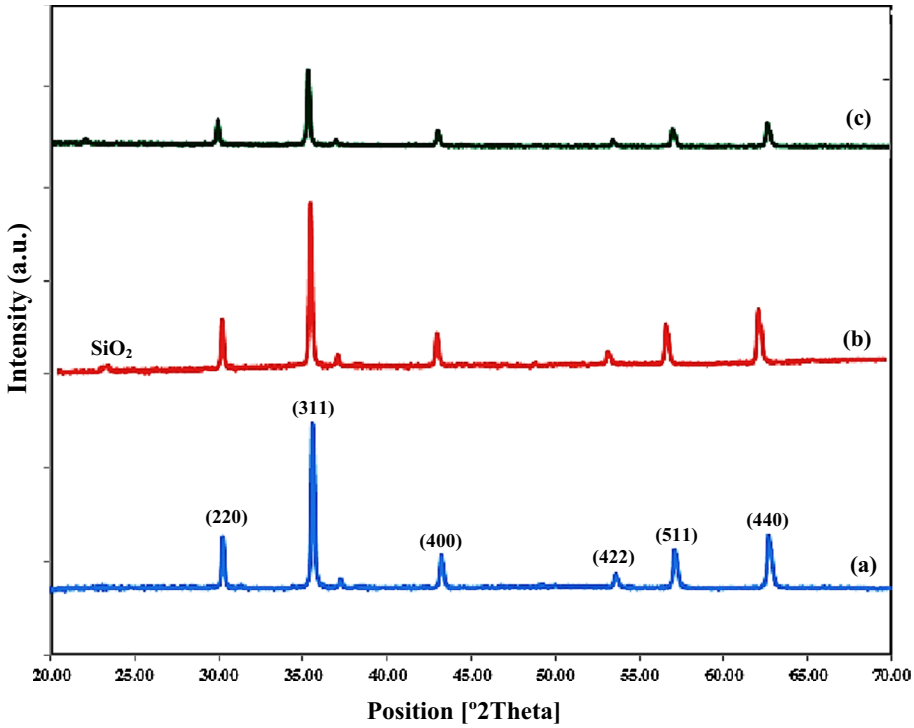


**Fig. 5** XRD pattern of the $Fe_3O_4$ (*a*), $Fe_3O_4$@$SiO_2$ (*b*) and $MoO_2$5CML–$Fe_3O_4$@$SiO_2$ (*c*)

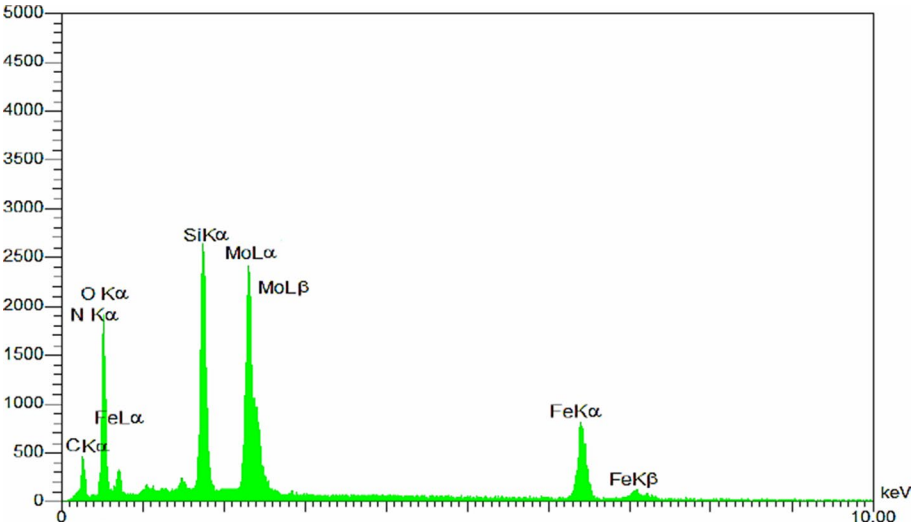


**Fig. 6** EDX analysis of $MoO_2$5CML–$Fe_3O_4$@$SiO_2$

with magnetic nanoparticles (Fig. 5a), which could be assigned to the shielding effect of silica on the surface of $Fe_3O_4$. It should be noted that the coating process did not induce any phase change of $Fe_3O_4$ during the preparation procedure [39].

## EDX studies

EDX analysis of $MoO_2$5CML–$Fe_3O_4$@$SiO_2$ nanocatalyst is depicted in Fig. 6, demonstrating the presence of C, O, N, Mo, Fe and Si. The results obviously confirm that the reaction between Schiff base complex and amine groups on the surface of the $Fe_3O_4$ nanoparticles occurred successfully.

## SEM images

The morphology, core–shell features and diameter of the precursors and catalyst were examined by SEM (Fig. 7) [14]. As shown in Fig. 7a, most of $Fe_3O_4$ nanoparticles are approximately spherical in morphology with a diameter of 30–40 nm, which is in good agreement with calculated

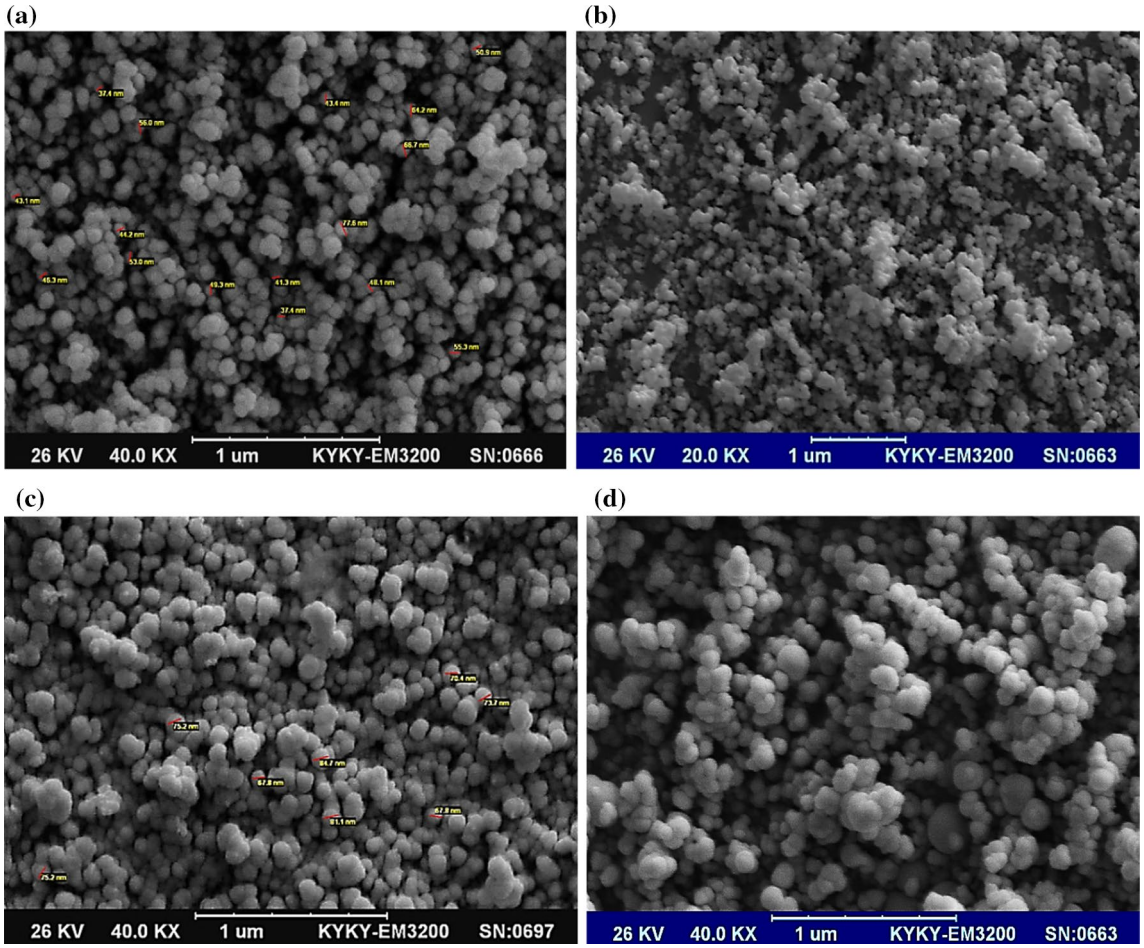


**Fig. 7** SEM images of the $Fe_3O_4$ (**a**), $Fe_3O_4$@$SiO_2$ (**b**), $MoO_2$5CML–$Fe_3O_4$@$SiO_2$ (**c**) and recycled nanocatalyst after 10th run (**d**)

value by Debye–Scherrer equation (36.3 nm). After encapsulation of $SiO_2$ through the sol–gel approach, $Fe_3O_4$@$SiO_2$ exhibited a uniform diameter of 50–60 nm (Fig. 7b). After anchoring Schiff base complex on the surface of $Fe_3O_4$, the supported catalyst still exhibits the spherical morphology with slightly larger particle size of 90–100 nm (Fig. 7c). It is obvious that coating process and covalent grafting have not significantly influenced the spherical morphology.

## Catalytic performance

### Oxidation of sulfides to sulfoxides

The catalytic activity of the $MoO_2$5CML–$Fe_3O_4$@$SiO_2$ for the selective oxidation of sulfides in the presence of $H_2O_2$ as oxidant was investigated at room temperature, and the results are given in Tables 1 and 2. Selective oxidation of sulfur-containing organic molecules, such as sulfides, is one of the most important organic transformations. To this end, we selected the oxidation of thioanisole as representative for initial studies in order to obtain the optimization of various parameters including solvent, amounts of oxidant, reaction time, amounts of catalyst and temperature.

The effect of different solvents on oxidation of thioanisole reaction is presented in Fig. 8a. Significant yield and selectivity improvement were observed when solvent-free conditions was employed, which might be due to the blocking of active sites by solvent molecules. In general, in solvents with higher dielectric constants such as methanol, ethanol and acetonitrile, higher yield of the product is obtained in compared with nonpolar solvents (dichloromethane and toluene).

The amounts of $H_2O_2$ as oxidant in the oxidation of thioanisole at room temperature were tested, and the highest catalytic performance was observed using 2 mmol of $H_2O_2$ (Fig. 8b).

The effect of catalyst concentrations on the reaction is shown in Fig. 8c. As it is clear in this Fig., 1 mol% of catalyst was chosen as optimum with respect to reaction time and selectivity. Increasing the catalyst loading above

**Table 1** Oxidation of different sulfides by $MoO_2$5CML–$Fe_3O_4$@$SiO_2$ under solvent-free condition

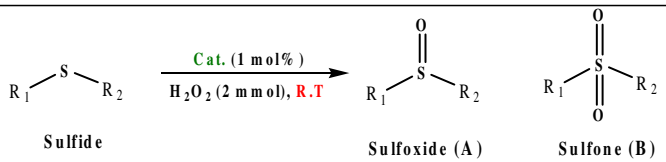


| Entry | Sulfide | Time (h) | Conversion (%) | *A* (%)[a] | *B* (%)[a] |
|---|---|---|---|---|---|
| 1 | 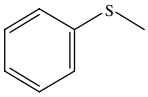 | 3:15 | 100 | 100 | 0 |
| 2 | 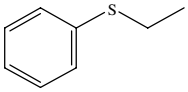 | 3:30 | 100 | 100 | 0 |
| 3 | 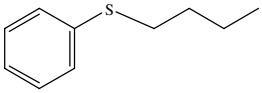 | 3:45 | 100 | 96 | 4 |
| 4 | 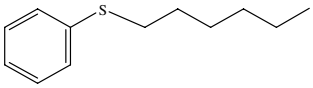 | 4:30 | 100 | 91 | 9 |
| 5 | 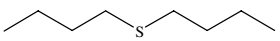 | 2:45 | 100 | 99 | 1 |
| 6 | 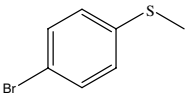 | 3:30 | 100 | 100[b] | 0 |
| 7 | 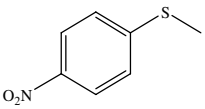 | 3:45 | 100 | 100[b] | 0 |
| 8 | 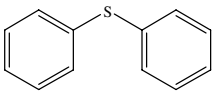 | 10:15 | 100 | 83[b, c] | 17 |
| 9 | 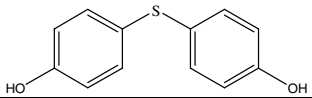 | 9:30 | 100 | 87[b, c] | 13 |

Reaction conditions: sulfide (1 mmol), $H_2O_2$ (2 mmol), catalyst (1 mol%), under solvent-free conditions, room temperature

[a] Determined by GC yield

[b] Determined by isolated yield

[c] For this case, solvent is ethanol

1 mol% decreases the reaction time and selectivity, and mixture of sulfoxide and sulfone is obtained.

To investigate the effect of the oxidizing agent, different oxidants such as $H_2O_2$, urea hydrogen peroxide (UHP), tert-butyl hydroperoxide (TBHP) and tetra-n-butylammonium oxone (TBAO) were employed in the oxidation reaction, and the results are presented in Fig. 8d. As it is obvious in this figure, $H_2O_2$ as eco-friendly oxidant exhibits highest selectivity and reaction conversion compared with other examined oxidants.

**Table 2** Oxidation of different sulfides to sulfones by $MoO_2$5CML–$Fe_3O_4$@$SiO_2$

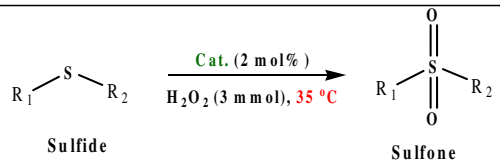


| Entry | Sulfide | Time (h) | Conversion (%) | Selectivity to sulfone (%)[a] |
|---|---|---|---|---|
| 1 | 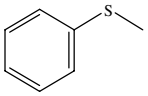 | 1:30 | 100 | 100 |
| 2 | 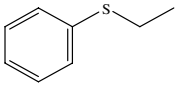 | 2:15 | 100 | 100 |
| 3 | 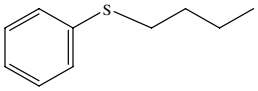 | 2:30 | 100 | 100 |
| 4 | 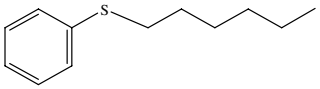 | 3:15 | 100 | 95 |
| 5 | 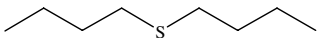 | 1:20 | 100 | 100 |
| 6 | 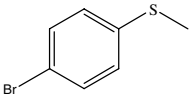 | 2:30 | 100 | 98[b] |
| 7 | 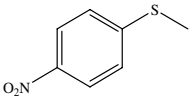 | 3:20 | 100 | 99[b] |
| 8 | 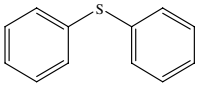 | 8:00 | 100 | 100[b] |
| 9 | 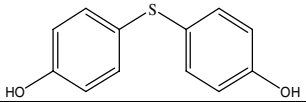 | 7:20 | 100 | 100[b, c] |

Reaction conditions: sulfide (1 mmol), $H_2O_2$ (3 mmol), catalyst (2 mol%), $CH_3CN$ (1 mL), 35 °C

[a] Determined by GC yield

[b] Determined by isolated yield

In the next step, the effect of temperature on the activity of the catalyst was studied (Fig. 8e). Room temperature was selected as optimized temperature with respect to reaction conversion and selectivity. Increasing the temperature to 40 and 60 °C, the selectivity between sulfoxides and sulfones is decreased.

To investigate the effects of catalytic active centers, background reactions were performed and the results are shown in Fig. 9. The oxidation reaction did not proceed using $Fe_3O_4$, $Fe_3O_4$@$SiO_2$, and $Fe_3O_4$@$SiO_2$–$NH_2$ as catalyst while if $MoO_2$5CML was used as catalyst oxidation reaction proceeded only in 55% conversion. Furthermore in

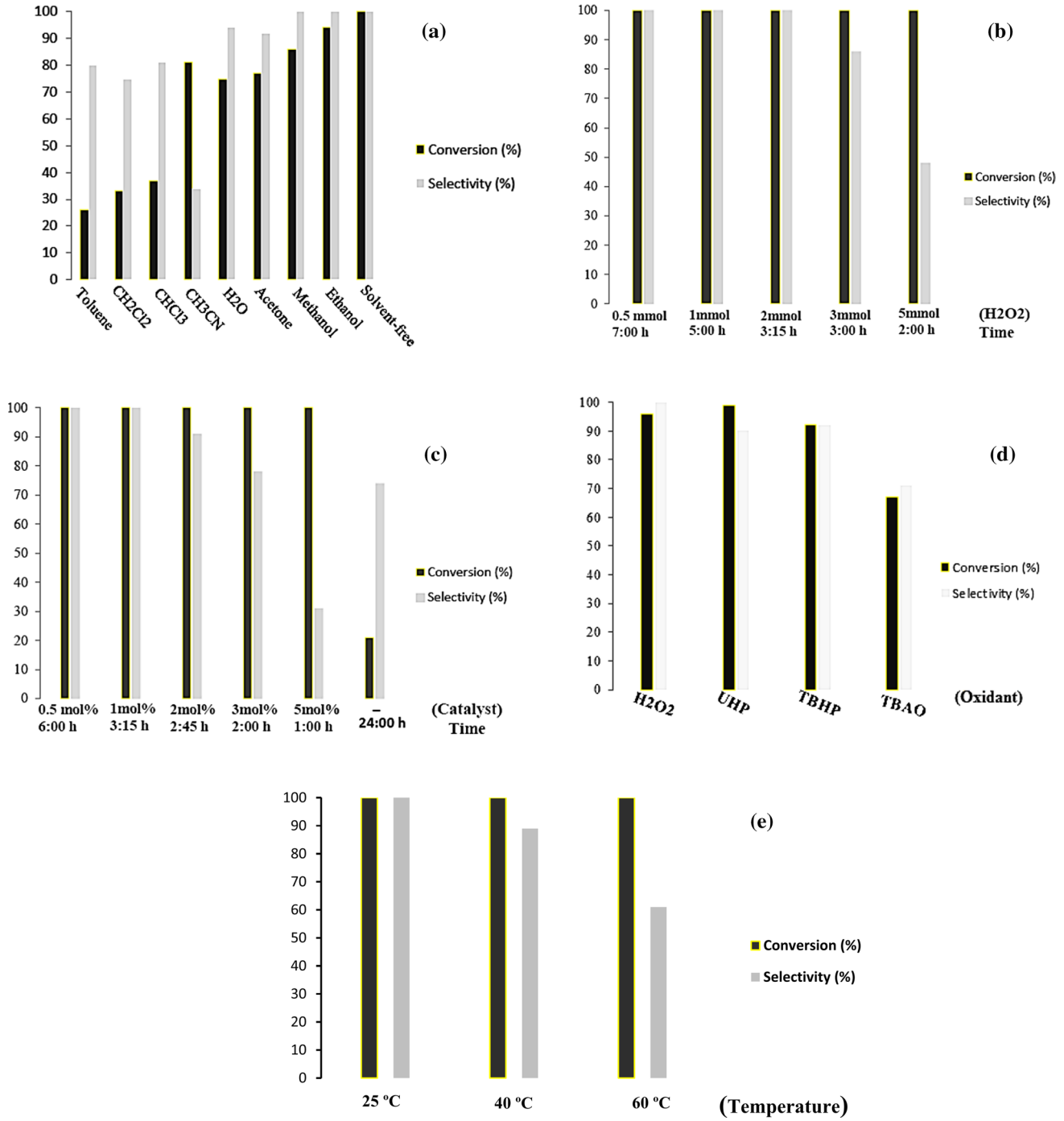


**Fig. 8** Optimization of the solvent nature (**a**), $H_2O_2$ (**b**), amounts of catalyst (**c**), different oxidant (**d**) and temperature (**e**) in the oxidation of thioanisole to the corresponding sulfoxide

the presence of $MoO_2$5CML–$Fe_3O_4$@$SiO_2$, the oxidation reaction occurred smoothly in 100% conversion with excellent selectivity. These results clearly show the role of Mo center in the oxidation reaction.

In order to find the general applicability of this catalytic system, after optimization of different parameters in oxidation of thioanisole (substrate: 1 mmol, catalyst: 1 mol%, $H_2O_2$: 2 mmol, reaction time: 3:15 h at room temperature), the catalytic activity of nanocatalyst was examined in the oxidation of various aromatic and aliphatic sulfides under the optimized reaction conditions, and the results are summarized in Table 1.

As it is clear in this table, phenylalkyl sulfides were oxidized selectively to their corresponding sulfoxides in

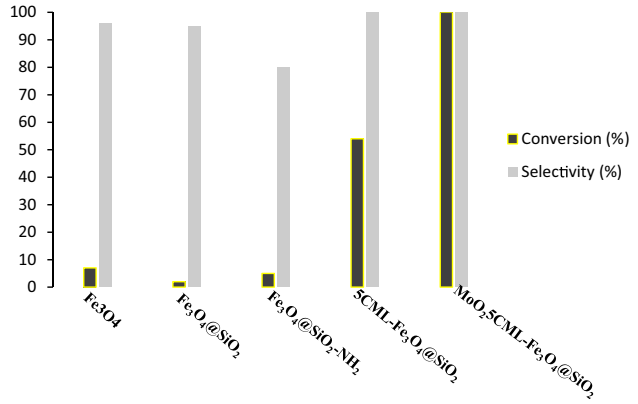


**Fig. 9** Background reaction in the oxidation of thioanisole

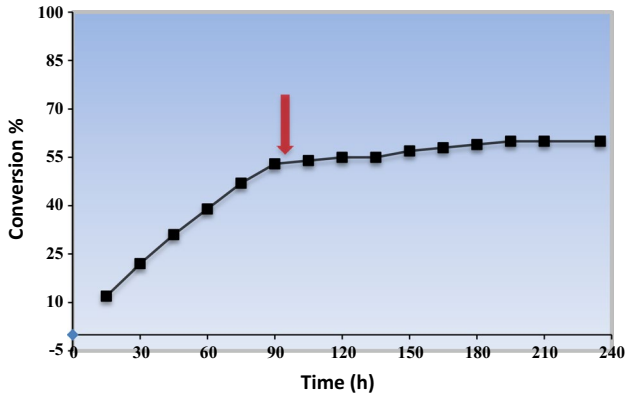


**Fig. 10** Hot filtration test for study of catalytic performance

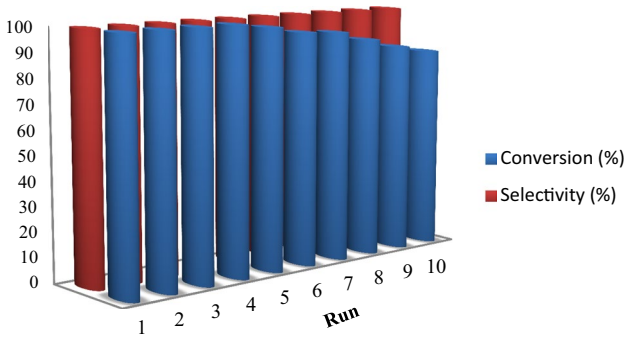


**Fig. 11** Reusability of catalyst for study of catalytic performance

excellent yields (Table 1, entries 1–4). Similarly, arylmethyl sulfides were oxidized smoothly to their corresponding sulfoxides (Table 1, entries 6 and 7).

Diaryl sulfides are shown lower reactivity in oxidation to their sulfides under optimal reaction conditions with slightly lower selectivity (Table 1, entries 8 and 9). This could be due to the steric hindrance of the diaryl groups. Dibutyl sulfide as a representative for dialkyl sulfides displayed excellent yield and selectivity to dibutyl sulfoxide (Table 1, entry 5).

In order to study the reaction mechanism, a catalytic run with optimized condition was performed in the presence of 2,6-di-*tert*-butyl-*p*-cresol (1 mmol) as a radical scavenger. The results showed that the conversion was reduced from 100 to 39% after 3:15 h (Table S1, entries 1 and 2 in supporting information) and reduced to almost 48% after 12:15 h (Table S1, entries 3–5). These results confirm that a radical pathway is more likely in the oxidation process [12]. The oxidation reaction was also carried out in the presence of imidazole (Table S1, entry 6), and conversation was reduced from 100 to 32%. It is probably due to the competition between oxidant and imidazole or the binding of imidazole as ligand to molybdenum metal center making the nanocatalyst inactive. The presence of unoccupied coordination sites on the molybdenum metal center of the catalyst is vital for its catalytic performance.

## Oxidation of sulfides to sulfones

Oxidation of thioanisole was chosen as a model reaction to investigate the effect of solvent, oxidant, catalyst loading and temperature on the reaction yield and selectivity. The results are summarized in Fig. S2 in supporting information. As it can be seen in this figure, optimization of reaction conditions for selectivity oxidation of thioanisole to the corresponding sulfone led to optimal conditions as: thioanisole; 1 mmol, $MoO_2$5CML–$Fe_3O_4$@$SiO_2$ as catalyst; 2 mol%, $H_2O_2$ as oxidant; 3 mmol, reaction time; 1:30 h, reaction temperature; 35 °C, $CH_3CN$ as solvent; 1 mL (Fig. S2(a–c)). The scope of the reaction was evaluated by employing different aromatic and aliphatic sulfides under the optimized reaction conditions, and the results are listed in Table 2. As it is clear in Table 2, various aromatic and aliphatic sulfides were efficiently oxidized to corresponding sulfones with good to excellent selectivity. It is interesting to mention that the presented catalytic system could selectively oxidize sulfides to their corresponding sulfoxides (Table 1) or sulfone (Table 2) under different reaction conditions.

## Hot filtration test

To verify the nature of heterogeneity or homogeneity of the catalyst, hot filtration test was carried out in the oxidation of thioanisole to its sulfoxide under optimal reaction conditions, and the results are presented in Fig. 10. Typically, after 90 min, the nanocatalyst was separated by external magnet and the filtrate was allowed to stir for additional 4 h and the reaction conversion was monitored by GC. The reaction conversion was 53% after 90 min and

**Table 3** Comparison of $MoO_2$5CML–$Fe_3O_4$@$SiO_2$ with various heterogeneous catalysts for selective oxidation of sulfides

| Entry | Catalyst (amount) | Oxidant | Solvent | Temperature | Time | Conversion (%) | Selectivity to sulfoxide (%) | Refs. |
|---|---|---|---|---|---|---|---|---|
| 1 | Mo complexes supported on silica (II) | $H_2O_2$ (2 mmol) | $CH_3CN$/MeOH (1:1) | −10 °C | 12 h | 100 | 92 | [40] |
| 2 | Silica-based tungstate (2 mol%) | $H_2O_2$ (3 mmol) | $CH_2Cl_2$/MeOH (1:1) | | 1.5 h | 99 | 82 | [41] |
| 3 | Fe(salen) complex (2 mol%) | $H_2O_2$ (1.5 mmol) | $H_2O$ | 20 °C | 3 h | 100 | 92 | [28] |
| 4 | $Na_2WO_4$, $C_6H_5PO_3H_2$, PTC (0.01 mmol) | $H_2O_2$ (10 mmol) | Solvent-free | 35 °C | 18 h | 100 | 99 | [42] |
| 5 | $Fe_3O_4$@$SiO_2$@ VO(salen) (10 mg) | UHP | $CH_2Cl_2$/MeOH (1:1) | r.t | 6 h | 99 | 95 | [12] |
| 6 | Au/CTN-silica (20 mg) | $H_2O_2$ (3 mL) | MeOH | 60 °C | 2 h | 100 | 94 | [43] |
| 7 | $Fe_3O_4$/salen of Cu(II) (50 mg) | $H_2O_2$ (0.5 mL) | EtOH | 60 °C | 3 h | 83 | – | [16] |
| 8 | Co@SiO2@[Mn(II) SBC] (40 mg) | $H_2O_2$ (1.17 mmol) | Ethyl acetate | 45 °C | 40 min | 100 | 92 | [44] |
| 9 | $MoO_2$5CML–$Fe_3O_4$@$SiO_2$ (1 mol% = 17 mg) | $H_2O_2$ (2 mmol) | Solvent-free | r.t | 3:15 h | 100 | 100 | This work |

59% after additional 4 h. This observation revealed that the leaching of the catalyst into the reaction mixture should be negligible, and the catalytic system in this reaction is truly heterogeneous.

### Reusability of the catalyst

The stability and reusability of the catalyst are of great importance, especially for green chemistry and commercial applications. Hence, the reusability of the catalyst was investigated under optimal conditions for oxidation of thioanisole to the corresponding sulfoxide. After completion of the reaction, the nanocatalyst was easily separated from the reaction mixture by an external magnet, washed with ethanol/$CH_2Cl_2$ 3 × 10 mL, dried in vacuum and reused directly in the subsequent runs (Fig. 11). The results depicted in Fig. 11 indicate that the nanocatalyst could be reused for at least 10 cycles without losing its catalytic activity and selectivity significantly.

The structure and morphology of the recycled nanocatalyst after ten cycles were examined by FTIR, SEM and VSM. FTIR spectrum of the recycled nanocatalyst after 10th run was similar to that of fresh catalyst and showed expected Fe–O, Si–O–Fe, Mo–O, C=N, aromatic C–H and aliphatic C–H vibration bands (Fig. S1). SEM images of the recycled catalyst after ten runs were very similar to those of fresh catalyst Fig. 7c, d, confirming that the morphology and structure of the nanocatalyst have been maintained during the recycling reactions. Furthermore, the used nanocatalyst after ten cycles showed superparamagnetic behavior and magnetization saturation value is about 33 emu $g^{-1}$ (Fig. 3d), which shows that there is no considerable change in its magnetic property. These observations reveal that $MoO_2$5CML–$Fe_3O_4$@$SiO_2$ can be used as an efficient recoverable and recyclable nanomagnetic catalyst in the selective oxidation of sulfides to their corresponding sulfoxides and sulfones.

The amount of molybdenum leaching was also investigated by ICP–AES analysis. The molybdenum leaching in the first and 10th runs was measured to be 0.5 and 3.3%, respectively (Table S2). It can be concluded from these results that molybdenum Schiff base complex is strongly bonded to the surface of $Fe_3O_4$@$SiO_2$–$NH_2$ nanoparticles and nanocatalyst is stable in the catalytic process because negligible metal leaching is happened.

In order to evaluate the performance and efficiency of our method, the catalytic activity of $MoO_2$5CML–$Fe_3O_4$@$SiO_2$ for selective oxidation of sulfides was compared with the several earlier reported heterogeneous catalysts in the literature (Table 3, entries 1–9). It is obvious that presented procedure in this work shows higher catalytic activity in terms of reaction time, reaction conversion, selectivity and temperature compared with other reported methods (Table 3, entries 1–8 and entry 9). The attractive features of the catalytic system in this method, such as stability, non-toxicity, low cost and simple recyclability and easy separation by external magnet, make it particularly suitable for oxidation reactions.

## Conclusion

In conclusion, we have developed a molybdenum Schiff base complex supported on $Fe_3O_4$ modified with silica as novel, efficient, recoverable and reusable nanocatalyst for the selective oxidation of various sulfides to their corresponding sulfides or sulfones under mild and green conditions. Oxidation of sulfides to sulfoxides was performed under solvent-free conditions at room temperature. However, oxidation of sulfides to sulfones was performed in $CH_3CN$ as solvent at slightly higher temperature (35 °C). Both sulfoxides and sulfones could be achieved with excellent selectivity by changing conditions in our catalytic system. The fresh and recycled catalyst after 10th cycles was characterized by different spectroscopic and microscopic techniques. The morphology and structure of catalyst were maintained after 10 recycles without any leaching of molybdenum confirming the stability of the nanocatalyst. The notable advantages of this work are use of green, cheap and nontoxic materials, good stability of nanocatalyst, high selectivity and facile reusability.

**Acknowledgement** The authors acknowledge the University of Mazandaran for financial support of this work.

## References

1. C. Han, J. Andersen, S.C. Pillai, R. Fagan, P. Falaras, J.A. Byrne, P.S.M. Dunlop, H. Choi, W. Jiang, K. O'Shea, D.D. Dionysiou, in *Sustainable Nanotechnology and the Environment: Advances and Achievements*, ed. by N. Shamim, V.K. Sharma (American Chemical Society, Washington, 2013), p. 201
2. D. Nath, P. Banerjee, Environ. Toxicol. Pharmacol. **36**, 997 (2013)
3. R.A. Sheldon, I. Arends, U. Hanefeld, *Green Chemistry and Catalysis* (Wiley, New York, 2007)
4. M. Tajbakhsh, M. Farhang, A.A. Hosseini, J. Iran. Chem. Soc. **11**, 665 (2014)
5. M. Perfezou, A. Turner, A. Merkoci, Chem. Soc. Rev. **41**, 2606 (2012)
6. A.K. Gupta, M. Gupta, Biomaterials **26**, 3995 (2005)
7. N.A. Frey, S. Peng, K. Cheng, S. Sun, Chem. Soc. Rev. **38**, 2532 (2009)
8. C. Sun, J.S.H. Lee, M. Zhang, Adv. Drug Deliv. Rev. **60**, 1252 (2008)
9. A.S. Teja, P.-Y. Koh, Prog. Cryst. Growth Charact. Mater. **55**, 22 (2009)
10. S. Laurent, D. Forge, M. Port, A. Roch, C. Robic, L. Vander Elst, R.N. Muller, Chem. Rev. **110**, 2574 (2010)
11. M.B. Gawande, Y. Monga, R. Zboril, R.K. Sharma, Coord. Chem. Rev. **288**, 118 (2015)
12. M. Bagherzadeh, M.M. Haghdoost, A. Shahbazirad, J. Coord. Chem. **65**, 591 (2012)
13. M. Esmaeilpour, A.R. Sardarian, J. Javidi, Appl. Catal. A Gen. **445–446**, 359 (2012)
14. R.K. Sharma, Y. Monga, A. Puri, G. Gaba, Green Chem. **15**, 2800 (2013)
15. L. Chen, B. Li, D. Liu, Catal. Lett. **144**, 1053 (2014)
16. A. Ghorbani-Choghamarani, B. Ghasemi, Z. Safari, G. Azadi, Catal. Commun. **60**, 70 (2015)
17. B. Karimi, F. Mansouri, H. Vali, Green Chem. **16**, 2587 (2014)
18. I. Fernández, N. Khiar, Chem. Rev. **103**, 3651 (2003)
19. J.P. Nehlsen, J.B. Benziger, I.G. Kevrekidis, Ind. Eng. Chem. Res. **42**, 6919 (2003)
20. P. Zhang, Y. Wang, H. Li, M. Antonietti, Green Chem. **14**, 1904 (2012)
21. A. Shaabani, A.H. Rezayan, Catal. Commun. **8**, 1112 (2007)
22. S. Davey, Nat. Chem. **2**, 604 (2010)
23. P. Le Maux, G. Simonneaux, Chem. Commun. **47**, 6957 (2011)
24. B. Karimi, M. Khorasani, ACS Catal. **3**, 1657 (2013)
25. B.S. Lane, K. Burgess, Chem. Rev. **103**, 2457 (2003)
26. C. Bolm, F. Bienewald, Angew. Chem. Int. Ed. **34**, 2640 (1996)
27. K. Kaczorowska, Z. Kolarska, K. Mitka, P. Kowalski, Tetrahedron **61**, 8315 (2005)
28. H. Egami, T. Katsuki, J. Am. Chem. Soc. **129**, 8940 (2007)
29. I. Sheikhshoaie, A. Rezaeifard, N. Monadi, S. Kaafi, Polyhedron **28**, 733 (2009)
30. A. Rezaeifard, I. Sheikhshoaie, N. Monadi, H. Stoeckli-Evans, Eur. J. Inorg. Chem. **2010**, 799 (2010)
31. Y. Wei, B. Han, X. Hu, Y. Lin, X. Wang, X. Deng, Procedia Eng. **27**, 632 (2012)
32. Y. Deng, D. Qi, C. Deng, X. Zhang, D. Zhao, J. Am. Chem. Soc. **130**, 28 (2008)
33. M. Masteri-Farahani, N. Tayyebi, J. Mol. Catal. A Chem. **348**, 83 (2011)
34. Z. Wang, B. Shen, Z. Aihua, N. He, Chem. Eng. J. **113**, 27 (2005)
35. J. Sun, G. Yu, L. Liu, Z. Li, Q. Kan, Q. Huo, J. Guan, Catal. Sci. Technol. **4**, 1246 (2014)
36. Y. Yang, Y. Zhang, S. Hao, J. Guan, H. Ding, F. Shang, P. Qiu, Q. Kan, Appl. Catal. A Gen. **381**, 274 (2010)
37. F. Nemati, M.M. Heravi, R.S. Rad, Chin. J. Catal. **33**, 1825 (2012)
38. D. Ma, T. Veres, L. Clime, F. Normandin, J. Guan, D. Kingston, B. Simard, J. Phys. Chem. C **111**, 1999 (2007)
39. R. Abu-Reziq, H. Alper, D. Wang, M.L. Post, J. Am. Chem. Soc. **128**, 5279 (2006)
40. F. Batigalhia, M. Zaldini-Hernandes, A.G. Ferreira, I. Malvestiti, Q.B. Cass, Tetrahedron **57**, 9669 (2001)
41. B. Karimi, M. Ghoreishi-Nezhad, J.H. Clark, Org. Lett. **7**, 625 (2005)
42. K. Sato, M. Hyodo, M. Aoki, X.-Q. Zheng, R. Noyori, Tetrahedron **57**, 2469 (2001)
43. F. Wang, C. Liu, G. Liu, W. Li, J. Liu, Catal. Commun. **72**, 142 (2015)
44. A.R.J. Azar, E. Safaei, S. Mohebbi, Mater. Res. Bull. **70**, 753 (2015)